YRHI-97-05

STAR NOTE 312

Yale Relativistic Heavy Ion Group

Brian Lasiuk

Department of Physics

Yale University

Brian.Lasiuk@Yale.edu

Particle Identification at STAR

Abstract

STAR is a large acceptance multi-purpose spectrometer that detects all charged particles produced in the pseudo-rapidity interval -2< η <2 with a Time Projection Chamber (TPC). A Silicon Vertex Tracker (SVT), located closer to the interaction region, covers the central region (-1< η <1). These detectors allow not only the trajectory of tracks to be reconstructed, but are also able to fix the 4-momentum by also measuring the specific energy loss of each track. Combining the ionization information from these detectors improves the quality and the range over which PID can be done by a single individual detector. A method which combines the ionization measurements from the two detectors, while having little dependence on the relative calibration of the detectors will be introduced and studied with simulated data.

1 Introduction

In the baseline configuration, STAR possesses the capability to perform Particle IDentification (PID) with the Time-Projection-Chamber (TPC) via the measurement of specific ionization or $\frac{dE}{dx}$. Using only the ionization information from the TPC, it is possible to extract the integrated number of a single particle species over a kinematic range of approximately 0.2-0.6 GeV/c with a reasonable degree of confidence by fitting a multi-Gaussian parameterization to the $\frac{dE}{dx}$ spectrum. However, the TPC does not provide enough power to discriminate between particles on a track-by-track basis. This is an important consideration because single track identification is required for event-by-event observables. PID utilizing specific ionization information is limited because of the statistical nature of the ionization process itself. Very large fluctuations in the amount of ionization produced over a given path length are possible. In fact the raw distribution of ionization produced along a track is not Gaussian at all, but rather Landau which is characterized by a long tail as shown in figure 1. This non-Gaussian behavior is due to high momentum transfer collisions which

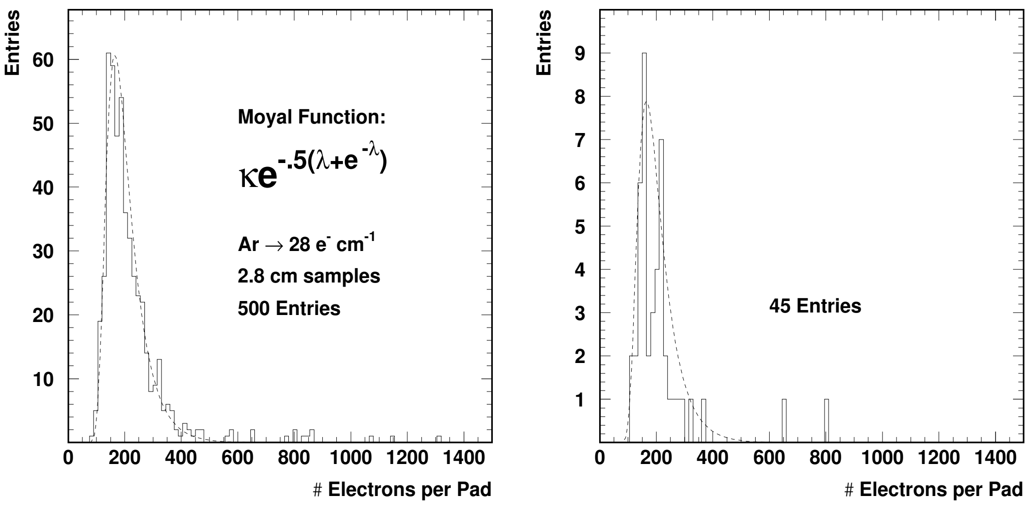

Figure 1: Ionization measurements of the same track with differing number of samples in Ar gas. The left panel shows 500–2.8 cm samples while the right panel shows only 45 samples, the maximum number available in the STAR TPC. The function shown with a dotted line is a very good approximation to a Landau curve—the Moyal function. Only the normalization κ is different between the two panels; λ is a parameter which is a function of the properties of the medium and the velocity of the charged particle.

produce high energy "delta" electrons. The ionization process can be modelled in terms of two components; primary and secondary interactions, which are shown schematically in figure 2. Primary ionization is due to direct processes between the charged particle and the medium, while secondary processes involve the subsequent interactions of the primary electrons.

The *total* number of interactions a charged particle has per unit length in a medium is

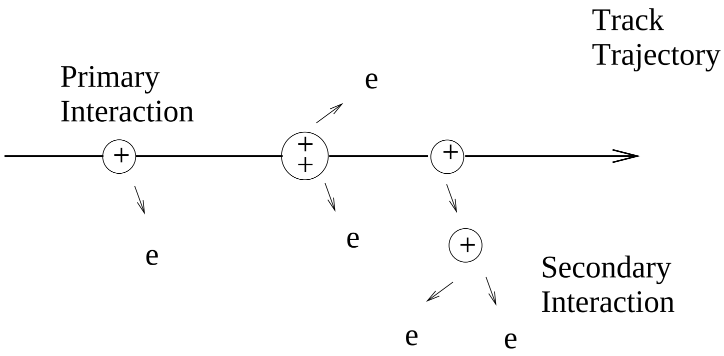

Figure 2: Schematic of ionization processes occurring along a track trajectory showing both primary and secondary ionization processes.

characterized by its mean free path, (α). The mean free path is inversely proportional to the electron interaction cross-section and the electron density of the medium. The number of encounters per path length L, is characterized by a Poissonian distribution with a mean of L/α. Of these interactions only a certain fraction transfer a sufficient energy to cause ionization within the medium.[1] Ionization produced in this manner is termed *primary ionization*. The energy transferred in the interaction is usually calculated by the conventional Rutherford scattering formula; that is, the energy dependence is given by E^{-n} where $n = 2$. If these primary electrons have a sufficient energy (i.e. above the ionization potential of the medium), they can produce additional ionization in subsequent interactions. This is known as *secondary ionization*. Because the E^{-2} distribution is not bounded, there is a significant possibility for producing high energy fluctuations. It is for this reason that the convolution of these two distributions produces a distribution with a Landau profile. It should be mentioned that the actual energy dependence (i.e. n) on the energy transfer is not medium independent. Measurements indicated that $n = 2$ is satisfactory in Ar but increases with decreasing Z of the medium. Such a dependence accounts for the fact that the resolution of ionization measurements is fairly independent of Z even though from pure counting statistics one would expect high Z gases to have better resolution [1].

Equation 1 is the conventional Bethe-Bloch equation which gives the rate of energy loss of a charged particle due to ionization in an homogeneous, isotropic medium:

$$-\frac{dE}{dx} = 4\pi N_o r_e^2 m_e c^2 \frac{Z}{A}\rho\frac{1}{\beta^2}z^2[\ell n(\frac{2m_e c^2}{I}\beta^2\gamma^2) - \beta^2 - \frac{\delta}{2}] \qquad (1)$$

where N_o is the Avogadro number, r_e ($= \frac{e^2}{m_e}$) is the classical electron radius, and ρ, Z, and A are the medium's density, atomic number, and mass number respectively, I is the ionization potential of the medium, z is the charge of the particle traversing the medium, and δ parameterizes a "density effect" of the medium which describes the saturation of the energy loss at highly relativistic velocities [2]. Figure 3 illustrates this graphically. In

[1] This fraction is not, in practice, calculable. For this reason the amount of energy deposited per electron-ion pair produced needs to be *measured* for each gas mixture.

the low energy region (i.e. $\beta\gamma$ <.5), the rate of energy loss is approximately proportional to β^{-2}.[2] As one approaches the region where $\beta\gamma$ ~1-3, all particle species go through a broad minimum at which the amount of ionization provides virtually no discriminating power among different particle species. As this region is passed, the ionization rate begins to increase roughly proportional to $\ell n(\beta\gamma)$ until $\beta\gamma$ reaches the order of 1000 at which point density (saturation) effects begin to dominate and the rate of ionization becomes constant. In a collider type experiment (as opposed to a fixed target where particles can carry a significant Lorentz boost along the direction of the beam) few particles, other than electrons, extend into the region of the relativistic rise. As such, the limitation faced is how to discriminate among particle species in the region near the minimum. The long Landau tail as a consequence of the high energy fluctuations coupled with a weak velocity dependence on the ionization yield is the reason for weak separation power via $\frac{dE}{dx}$.

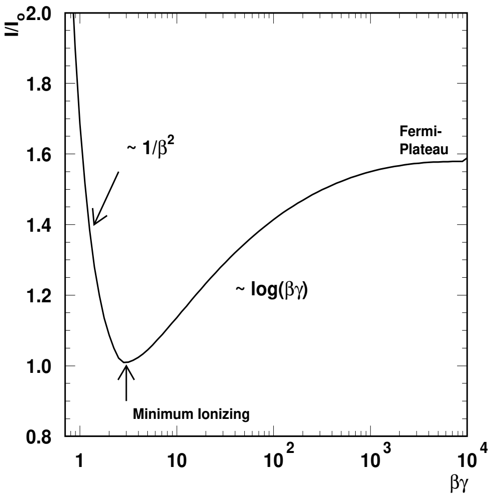

Figure 3: Rate of energy-loss for charged particles as given by equation 1. At a collider most hadrons will populate the region to the left of the minimum (i.e. $\beta\gamma < 3$).

Before going further, it should be noted that while theory allows for the somewhat empirical calculation of the rate of energy lost per unit length of a charged particle (see equation 1) a detector measures the energy *deposited* in a very localized volume. The assumption that these quantities are *directly* proportional is implicit in any attempt to do PID by specific ionization.

Given the ionization distribution of a single track as shown in figure 1, it is necessary to quantify some sort of average or mean value for the energy loss which accurately reflects its velocity. The *mean*, or arithmetic average and the *most probable*, or the maximum of the distribution, are two such quantities. They are shown schematically in figure 4. It is noteworthy that the two values are identical in the limit of a Gaussian distribution. In the case of a Landau distribution, the mean is extremely sensitive to the number of counts in the

[2]The functional dependence is somewhat better described as $\beta^{-5/3}$.

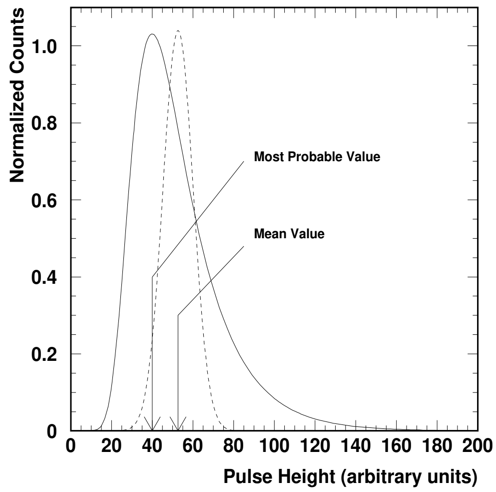

Figure 4: The Moyal function, an approximation to a Landau distribution, is shown with a Gaussian about the mean value of the distribution. The error on the Gaussian is that expected from N measurements.

tail of the distribution. For this reason the mean is very difficult to understand quantitatively with high precision because it is not only very sensitive to the exact dependence of the energy transfer, but also to the efficiency that a detector can measure and associate these delta electrons with the parent track. This implies that the mean can be rather difficult to quantify to a high precision, especially in the case of thin detectors where high energy secondaries can escape the active region! In order to reduce the effect of the high energy deltas, several methods which suppress the contributions of the Landau tail in characterizing a mean value have been used previously.

The simplest method to suppress the contribution of the tail is to use a logarithmic mean as defined by equation 2 [3]:

$$< \frac{dE}{dx} >= \exp\left(\frac{1}{N}\sum_{i=1}^{N}\ell n(Q_i)\right) \tag{2}$$

where N is the number of ionization samples on the track and Q_i is the amount of charge in the i^{th} sample. It is computationally fast however, the tail suppression is a rather weak in this method and there is still a large sensitivity to the number of counts in the region of the high energy tail. For this reason it is much more reliable to quantify the *most probable* value. This can be estimated by truncating a fixed fraction of the charge samples in order to give the distribution a Gaussian profile and calculating the mean of the remaining values. Such a method is referred to as the "truncated mean" [4]. One drawback however, is that much of the data is unused in the calculation. This is addressed with the more sophisticated maximum likelihood analysis, but it introduces a higher computational expense which is a concern when a single event has on the order of 10,000 tracks. Allison and Cobb first suggested a method which compares the distribution of the ionization measurements to reference distributions and assigns a statistical probability that the two match [5]. This method is more accurate because it utilizes both the numerical values of the energy loss *AND* the shape of the distribution in assigning PID. However, it requires a large number of samples (i.e. >200) so the profile of the measured ionization distribution is defined with a reasonable precision such that comparisons with reference distributions can be assessed via reliable quantitative methods (i.e. χ^2). To give an idea of the number of samples required, it is instructive to refer back to figure 1 which illustrates two different distributions characterizing the same track—one with 500 samples while the other has only 45, the number of pad rows in the radial direction of the STAR TPC. It is unlikely that a meaningful quantitative comparison (i.e. using a χ^2 or other suitable test) could be made between a reference distribution and the one with only 45 samples. For these reasons, the truncated mean method is the most common algorithm used in experiments.

The truncated mean is characterized by a truncation ratio (a:b) which determines the fraction of the lowest (a) and the highest (b) values which are to be kept for the calculation of the most probable value. They are determined experimentally by optimizing (i.e. minimizing) the resolution, R $(= \sigma(\frac{dE}{dx})/ < \frac{dE}{dx} >)$.

Figure 5 shows the resolution as a function of the number of charge samples for various truncation ratios. Although there are slight variation with different materials, the ratio is

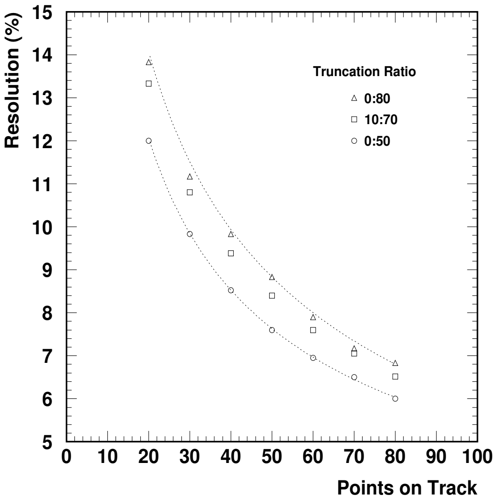

Figure 5: Expected Resolution as a function of the number of points on a track for several truncation ratios. A broad minimum between the ratios of 0:40-0:60 occurs and considerations of stability of the cuts with varying number of points become deciding values in the final optimization. The curves are a guide to the eye.

generally optimal in the range where the top 60% (0:40 truncation ratio) to the top 40% (0:60) of values are dropped. The logarithmic mean method generally gives a resolution which is 2-3% worse than the truncated mean method with an optimized truncation ratio. In the remainder of this note, the logarithmic mean will be used as it serves to quantify a very conservative estimate for the resolution to be obtained at STAR.

Several authors have deduced empirical expressions for expected resolutions of the mean (most probable) ionization value in gaseous mediums. It should be noted that there is a slight dependence on the resolution of the $\frac{dE}{dx}$ depending on the method used to quantify this value. For example Walenta parameterized the resolution of the energy loss attained utilizing the truncated mean method (with a 0:40 ratio) as [6]:

$$R = \frac{\sigma(\frac{dE}{dx})}{<\frac{dE}{dx}>} = .47(P \cdot D)^{-.32} N^{-.43} \tag{3}$$

where P is the pressure of the gas (in atm), D is the sample length (in cm), and N is the number of samples. The resolution of ionization measurements quantified with the maximum likelihood method was parameterized for any general medium by Allison and Cobb as [7]:

$$R = \frac{\sigma(\frac{dE}{dx})}{<\frac{dE}{dx}>} = .34(\xi/I)^{-.32} N^{-.46} \tag{4}$$

where ξ/I is given numerically as 6.83νxP/Iβ^2 where ν is the mean number of electrons per molecule ($\sim$17.2 for $ArCH_4$ (90/10)), x is the length of the sample (in cm), P is the pressure (in atm) and I is the ionization potential (in eV). It is noteworthy that the dependence of the resolution on the number of samples N, in both equations 3 and 4 differs from $\sqrt{N}$ that would be expected from Gaussian statistics. However, the resolution obtained from the maximum likelihood method (equation 4) most closely approximates Gaussian statistics.

Although resolution is easy to quantify, the real figure of merit is the separation power or how well one is able to distinguish between different particle species. In order to quantify the separation power it is useful to define an expression S, as the difference of the means of two distributions divided by the width of the distributions as follows:

$$S = \frac{<\frac{dE}{dx}>_1 - <\frac{dE}{dx}>_2}{max(\sigma_1, \sigma_2)} \tag{5}$$

The separation power is maximized when σ becomes small and it can be seen that in both equations 3 and 4, the width decreases with increasing number of samples. Thus it is fixed for the STAR TPC where the number of pad rows is 45. Equation 3 predicts a resolution of $\sim$8% which is sufficient to identify particles in the low energy region (**p**<0.4 GeV/c) but marginal as the region of the minimum is approached. A more quantitative treatment will be presented in section 2.1.

2 PID from Multi-Detector Systems

STAR has the capability to make specific ionization measurements in several different detectors. The Silicon-Vertex-Tracker (SVT), like the TPC, measures not only position but also ionization produced by charged particles. The problem is how to combine the two different measurements to maximize the separation power.

The CERN experiment NA49 has a similar problem of how to combine several ionization measurements, although all detectors (4 in total) involved are TPCs. In order to extract PID information from the TPCs, the ionization information from two different chambers is plotted against each other. In the case of Gaussian statistics where the detectors are the same and a linear relation between the energy loss in all chambers exist, the dispersion (separation power) is increased by a factor of $\sqrt{2}$ by defining a cut in 2 dimensions. Deviation from Gaussian statistics reduces this marginally. An example is shown in figure 6 where the $\frac{dE}{dx}$ measurements in two different TPCs for particles in the momentum range between 4-15 GeV/c are plotted against each other. Even in the rather large momentum range the electrons, pions and protons are separated to an extent that PID on a track-by-track basis can be carried out. Although the same increase in separation would result in the case where

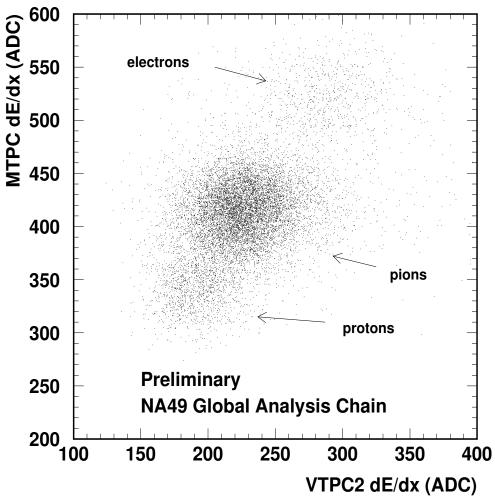

Figure 6: The correlation between $\frac{dE}{dx}$ in MTPC and VTPC2. These are preliminary results from the NA49 "Global Chain".

the ionization values measured in each detector were simply averaged [8], complications from the absolute calibration are introduced even when combining similar detectors. For example, if a linear relation exists in the energy loss between different chambers, one expects that the same Bethe-Bloch parameterization (up to a constant) will describe the energy loss. This is not the case at NA49. The reasons are several fold—most importantly being that (i) different gases are used in different detectors, (ii) each detector has a different sample length, and (iii) the presence of a magnetic field in two of the chambers (VTPCs). Because of such differences it is not appropriate to simply compute the average. Rather, it is necessary to deduce the absolute energy loss from each detector and combine them with the appropriate weighting taking into account differences in medium properties, sample lengths, resolutions, differences in the environments (i.e. magnetic field), etc., some effects of which are very difficult to estimate quantitatively.

By plotting two independent measurements of the ionization versus each other, the dependence on the cross calibration between different detectors is virtually eliminated [9]. This is especially important if the ionization properties of the chamber gases are not well understood.

2.1 Combining Si and Ar $\frac{dE}{dx}$ Measurements at STAR

The profile of the Bethe-Bloch curve in Si and Ar (or other high Z noble gas) differs because of the different properties of the media. These are summarized in table 1. In fact, it will be shown that these different properties aid in the separation of particle species.

Comparison between Si and Ar					
Medium	Number of Samples	Sample Length cm	X_o (%)	Density g cm^{-3}	dE/dx (e^-/cm)
Si	3	.03	.321	2.33	2.12×10^7
Ar	45	2.7	.025	.00178	28

Table 1: Properties of materials used in STAR for $\frac{dE}{dx}$ information.

The SVT has only 3 active layers but the amount of material in a single layer is much more than the TPC (by an order of magnitude). One 300μm layer of Si is .32% of a radiation length whereas a single sample in the TPC (a pad length of Ar) is $\sim$.025%. A consequence of this is that particles lose considerably more energy due to bremsstrahlung within the Si than the gas. Although the energy loss due to bremsstrahlung is not measured, it illustrates that the physics processes are different in the two media. Figure 7 shows the measured $\frac{dE}{dx}$ quantified by the logarithmic mean method in both the SVT (left panel) and the TPC (right panel) for equal populations of electrons (e), pions (π), kaons (K), and protons (p) in the momentum range from $0.6<p$ (GeV/c)<0.7. Because of the small number of layers remnants of the Landau tail are more visible in the Si measurements than the gas, however, because of the relatively large amount of material in the SVT, the effect of statistical fluctuations in the ionization process are reduced and the resolution is comparable to that extracted from 45 samples in the TPC gas. Although it is possible to see slight separation in both cases, and particle yields could be estimated in ensembles of events using multi-parameter fits to the distribution, neither system by itself is sufficient to do PID on a track-by-track basis which is critical for the physics goals of STAR. The resolution obtained from these distributions are shown in table 2. It should be noted that the resolutions from the STAR TPC using an optimized truncated mean (or other suitable) method should be significantly better (i.e. of the order of 8%). This will have the effect of reducing the long tails of the distributions which should allow tighter cuts to be made. As a first attempt, using conservative numbers should allow for reasonable estimates of real performance. For example there will be a complication in combining the $\frac{dE}{dx}$ measurements from the inner and outer regions of a super-sector in the TPC because of the difference in pad lengths. Although this is possible to do, there may be a reduction in the expected resolution that has not been incorporated into this simulation.

The simplest way to combine the measurements from the two systems is an arithmetic average as outlined before, but there are two specific concerns with this: (i) the large difference in the amount of energy lost per unit length in the two materials and (ii) the fact that the energy loss mechanisms are slightly different in Si and Ar. An example of this is shown in figure 8 which is the momentum dependence of the ionization. The ratio of the minimum to the height of the plateau in Si is only of the order of 1.1 as compared to Ar which is 1.6.

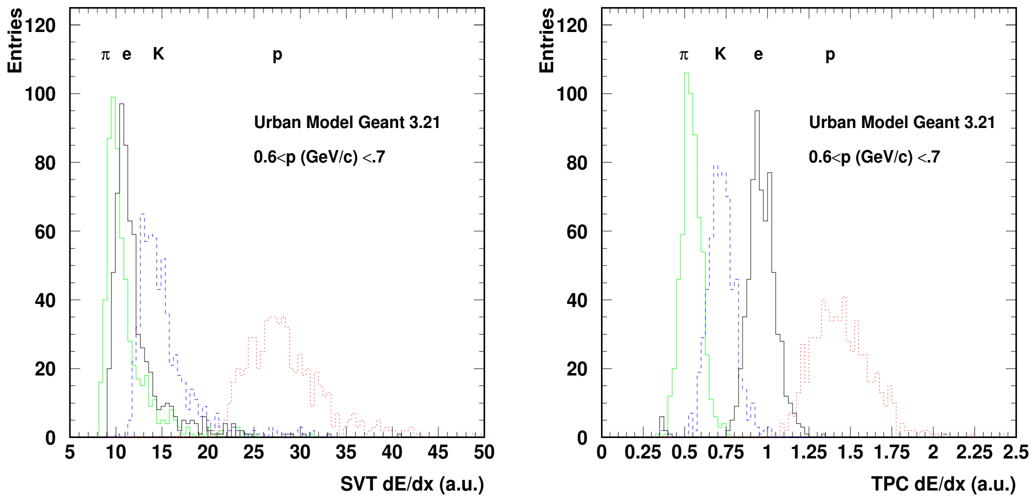

Figure 7: Distribution of the energy loss given by the logarithmic mean method for tracks that traverse the 3 SVT layers and the 45 TPC pad rows in the momentum range from 0.6<p (GeV/c)<0.7. The same number of electrons, pions, kaons, and protons are contained in each distribution. Although this does not reflect the particle composition in a real event, this illustrates that a 1-D projection is insufficient to realize PID on a track-by-track basis, even in a moderate momentum region.

If a similar technique to that employed by NA49 is used, a cut in a two-dimensional space can be defined that is effective in separating particle species without relying heavily on an absolute calibration. The result for STAR is illustrated in figure 9. The left panel shows the correlation of the data from figure 7 in two dimensions. This demonstrates that simultaneous use of the $\frac{dE}{dx}$ information from the two detectors can extend the range over which PID can be done significantly. A series of plots over the momentum region from 0.2<p (GeV/c)<2.1 is contained in Appendix A. It should be noted that this method places a premium on the efficiency of track matching between the two detectors.

Perhaps more impressive is that the electron-hadron (e/h) separation is extended significantly to higher momentum. This is shown in the right panel of figure 9, where electrons are cleanly separated from the hadrons even in the momentum range from 1.6<p (GeV/c)<1.8. Such a separation exists because of the different profiles of the Bethe-Bloch curve in the two media and the fact that the particles populate the β^{-2} region. For example, referring to figure 8, which is the form of the energy loss curve for charged particles in the context of the Urban model in GEANT, the height of the rise is only a factor 1.1 above the minimum in Si, but a factor 1.6 in the TPC gas.[3] Therefore, the kaon (and proton) energy loss remains above the plateau in Si at energies up to 1 GeV/c but falls below it in Ar. Because even electrons of moderate energy are highly relativistic, their energy loss is always in the saturated region of the plateau, independent of their momentum or the medium. In effect,

[3]This is not a feature of GEANT but rather reflects that the height of the relativistic rise generally decreases with increasing density.

dE/dx Resolution in Si and Ar								
	Ar				Si			
Momentum (GeV/c)	e	π	K	p	e	π	K	p
.3-.4	7.4	10.8	18.9	12.1	11.6	11.0	15.8	16.9
.4-.5	7.5	11.2	13.4	12.6	9.5	13.0	13.4	13.7
.5-.6	8.2	10.7	11.0	12.8	10.3	9.7	12.8	11.6
.6-.7	8.0	10.8	10.3	11.5	9.7	10.7	11.2	11.3
.7-.8	8.1	10.9	11.3	11.0	9.4	9.1	8.9	13.0
.8-.9	8.2	10.8	11.3	10.0	9.2	8.5	8.8	10.2
.9-1.0	7.7	10.2	10.7	10.7	13.1	10.0	11.2	9.3

Table 2: $\frac{dE}{dx}$ resolutions in per cent in the STAR SVT and TPC.

Si and Ar are complimentary because when different particle species have an overlapping energy loss in one material, the other medium provides some separation power. For example, the kaon ionization yield is equal to the electron ionization yield at 0.4 GeV/c in Ar, but at 1.1 GeV/c in Si. This is seen in the vanishing e/K separation power in the TPC at 0.4 GeV/c in table 3. Thus although the two particles would be indistinguishable in the TPC, the SVT allows some degree of separating power. In the case of pions and kaons, the

Separation Power					
	Momentum (GeV/c)	e/K	e/π	π/K	K/p
TPC	.2-.3	2.87	4.53	3.48	1.50
	.3-.4	1.75	5.53	3.34	4.81
	.4-.5	.42	5.66	3.68	4.94
	.5-.6	1.52	5.23	3.13	4.62
	.6-.7	3.00	5.23	2.56	4.10
	.7-.8	3.95	5.27	1.39	3.90
	.8-.9	4.47	5.28	.89	.50
SVT	.3-.4	2.81	.35	2.88	-
	.4-.5	3.59	.54	3.84	4.59
	.5-.6	2.81	.84	3.26	4.31
	.6-.7	2.23	.81	2.81	4.11
	.7-.8	1.40	1.06	2.71	4.49
	.8-.9	1.37	1.08	2.38	3.48

Table 3: Separation power as defined in equation 5 for the TPC and SVT.

separation power goes down dramatically at 0.7 GeV/c in the TPC while it is still significant in the Si. The decrease in separation power is a result of all the hadrons approaching the region of the broad minimum. At this point ionization yields are identical, independent of

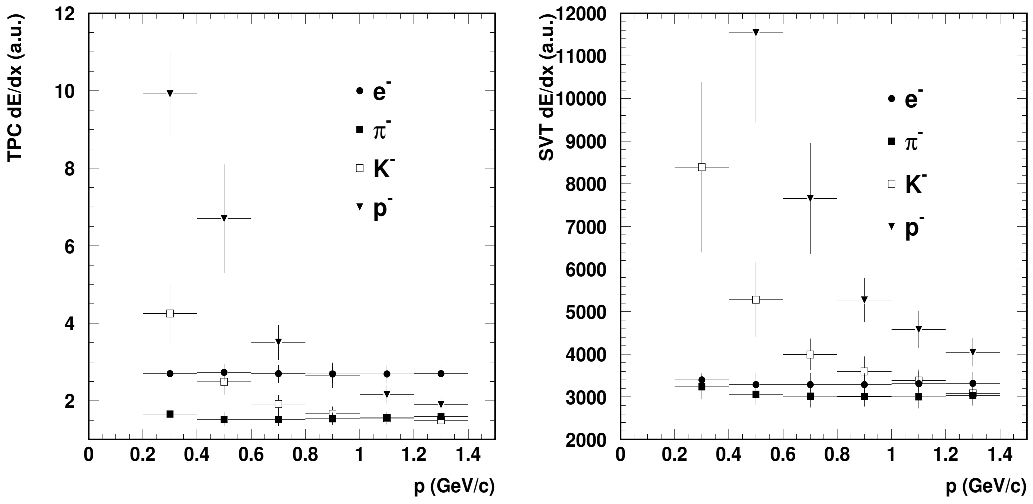

Figure 8: The $\frac{dE}{dx}$ in the SVT and TPC as described by the Urban model in GEANT. The error bars on the momentum axis span the momentum range utilized while the vertical error bars denote 1 σ.

particle species. This can be seen graphically in figure 9 where all the different hadrons populate the same region. Although this means that K/π (or any hadron) separation will require some additional hardware system to extend identification beyond 0.8-1.0 GeV/c, current simulations suggest that the TPC-SVT system is capable of separating electrons from hadrons beyond 2 GeV/c. This is a consequence of the minimum being rather broad. The separation begins to degrade once the pion ionization starts moving upward in the relativistic rise which begins at ~2.5 GeV/c.

It should be noted that this separation would not be realized if the relative height of the plateau to the minimum was identical in both media. Furthermore, if the height of the rise in the gas was smaller, the separation power would also decrease. In light of this, the use of HeC_3H_8 (50/50) in the STAR TPC would compromise the PID capabilities as the height of the plateau is only 1.4 above the minimum. However due to the fact that it is a lower Z, it produces a smaller amount of ionization which would result in a smaller amount space charge within the chamber volume which makes it very attractive for chamber operations.

2.2 Particle Separation

Up until this point, the separation between particle species has been illustrated using very generic events with equal numbers of all particles (e, π, K, and p) distributed flatly in pseudo-rapidity and transverse momentum. The restriction in pseudo-rapidity space was made to be -1< η <1 because it is the limit of the SVT acceptance. The identification capabilities do not seem to be seriously degraded when a more realistic particle composition is utilized. For example figure 10 shows the separation of particles from an event where there are 7000 pions, 5000 electrons, 1000 kaons, and 500 protons, and the results are quite

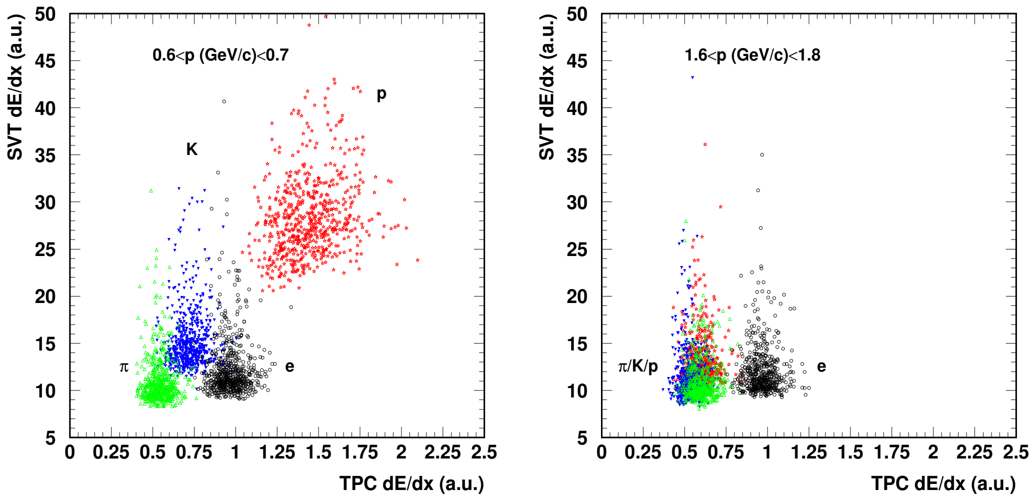

Figure 9: Data from the one-dimensional plots in figure 7 plotted versus each other. The left frame illustrates that particle separation (even K/π) is possible at momenta up to 0.7 GeV/c. The right frame shows that even though hadronic separation is severely degraded at high momenta, electron/hadron separation is still feasible.

similar, even when the pion signal is much larger than the other particle populations.

The previous figures have shown separation for generic events in a very qualitative way. Similarly table 1 shown the separation power as defined by equation 5, but this is not an observable. The real observable is the efficiency of the identification versus the contamination of other particle species. This is shown in a quantitative manner in figures 11 and 12.

The left panel in figure 11 shows the efficiency of the electron identification, using very simple cuts that define the electron region in the two dimensional space as illustrated in figure 9. The decrease in efficiency, due to the tighter cuts, in the regions where the energy loss of the protons and kaons becomes equal to that of the electrons is accompanied by an increase in the contamination. However, because the SVT still provides a sizable separation power, there is still a possibility to discriminate between the electrons and the hadrons with a reasonable efficiency (i.e. >85%). The high contamination at the crossing point can be reduced substantially with tighter constraints on the ionization cuts, but this results in a significant reduction in efficiency—to the 60% level. It is noteworthy that the contamination in the electron sample is dominantly protons and kaons in the low momentum region rather than pions. The reason is the energy loss of the pions is in the region of the minimum and is separated from the mean energy loss of the electrons by a factor of ~1.6. Only in the momentum range above 2.5 GeV/c, when the energy loss of the pions begins to move up the relativistic rise do they become a significant contaminant.

Shown in the right panel of figure 11 is the same type of plot for the protons. As the energy loss of the protons moves down the β^{-2} part of the Bethe-Bloch curve and into the region of the minimum, the contamination increases substantially. This is at approx-

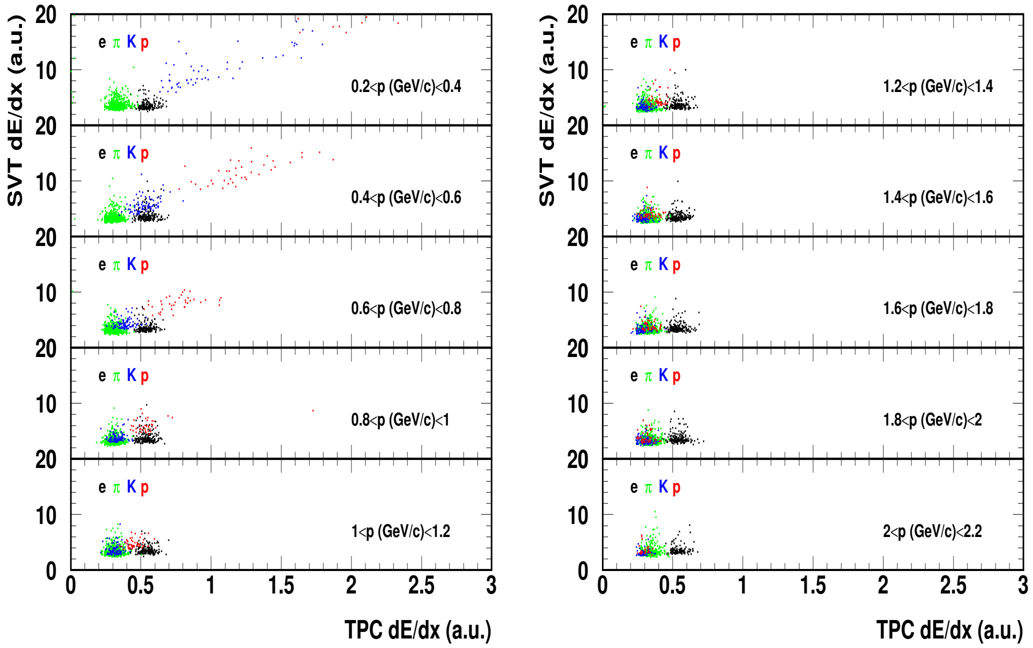

Figure 10: Particle separation is very similar when a particle composition very similar to that expected in a single event is analyzed.

imately 1.0 GeV/c. Again, in the momentum region around 0.5 GeV/c, the electrons are the most worrisome contaminant. It should be reiterated at this point that the resolution of the $\frac{dE}{dx}$ measurements in the STAR detector are expected to be of the order of at least 2% better with the use of the truncated mean or maximum likelihood method. This *should* improve identification capabilities further. Unlike the electrons however, the identification possibilities of the protons at higher momentum (i.e. >0.7 GeV/c) deteriorate because the region of the minimum, where all particle species produce very similar ionization yields is approached. In this region the most significant contaminant for protons is the kaons. In fact the reason the electrons get cleaner in this region is that the ionization of the protons decreases (moving away from the mean electron ionization) because it is moving down the β^{-2} part of the Bethe-Bloch curve.

The analogous plots to figure 11 for pions and kaons are shown in figure 12 which are not as encouraging as the electron and proton identification possibilities. Although the integrated yield of pions and kaons can be estimated by a simultaneous fit to the "Gaussians" of figure 7 up to momenta of ~1 GeV/c, figure 12 does not suggest that π/K separation will be possible at momenta greater than 0.8 GeV/c with a reasonable efficiency using ionization information from the SVT and TPC systems. This is the main motivation for the addition of an auxiliary detector system.

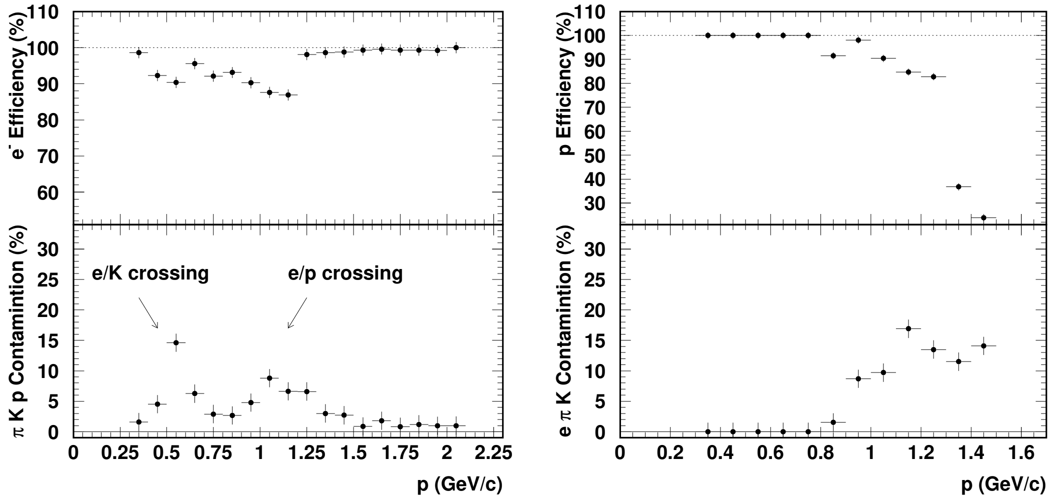

Figure 11: Electron and proton identification efficiency with the associated contamination in momentum bins of 0.1 GeV/c. Efficiency is defined as the number of particles identified over the total number. Contamination refers to number of misidentified particles in the sample over the total sample size.

3 Summary

Considerations of various methods to quantify specific energy loss were outlined and the logarithmic mean method was used to illustrate an approach that combines the ionization information from the Silicon Vertex Tracker (SVT) and the Time Projection Chamber (TPC) in order to carry out Particle IDentification (PID). Because of the different profiles of the Bethe-Bloch curves which parameterize energy loss due to ionization as a function of momentum (or velocity), the two devices are quite complimentary and allow a simple means to carry out track-by-track identification. Perhaps a somewhat surprising result is the power of the TPC/SVT in e/h separation, and in particular the e/π separation which extends up to 2.5 GeV/c. This is an evolving document and as always, comments, suggestions, etc. are welcome at Brian.Lasiuk@Yale.edu.

References

[1] B. Lasiuk *Particle Identification in the NA49 TPCs*, presented at the 7^{th} Pisa Meeting on Advanced Detectors, May 25-31, 1997 Elba, Italy. To appear in *Nuclear Instruments and Methods.*

[2] E. Fermi, Phys. Rev. **57** (1940) 485.

[3] A. I. Alikhanov et al., *Proc. CERN Symposium on High Energy Accelerators and Pion Physics*, **2** (1956) 87; (CERN 56-25).

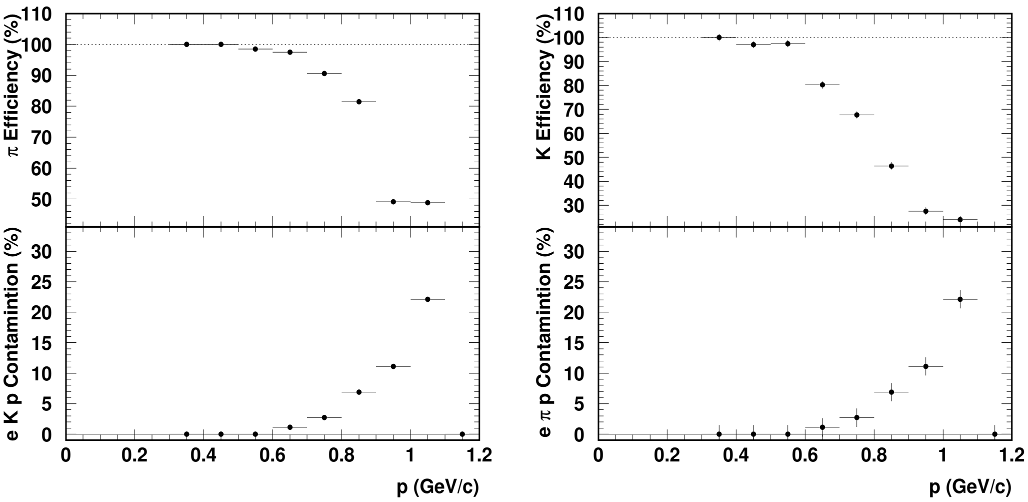

Figure 12: Pion and kaon identification efficiency with the associated contamination in momentum bins of 0.1 GeV/c.

[4] G. Igo and R. M. Eisberg, Rev. Sci. Instr. **25** (1954) 450, and more recently, I. Lehraus et al., NIM **153** (1978) 347.

[5] see W. W. M. Allison and P. R. S. Wright, *The Physics of Charged Particle Identification: dE/dx, Cerenkov and Transition Radiation* in Experimental Techniques in High-Energy Nuclear and Particle Physics. T. Ferbel ed., (New York Plenum : 1990).

[6] A. H. Walenta et al. NIM **161** (1979) 45.

[7] W. W. M. Allison and Cobb, Ann. Rev. Nucl. Part. Sci, **30** (1980) 253.

[8] H. Wieman, private communication.

[9] B. Lasiuk, PhD. thesis UCLA, 1997, (unpublished).

A Particle Separation

Shown in the following plots are the particle separations as given by the two tracking detectors in Δp=0.1 GeV/c momentum bins ranging from 0.2<p (GeV/c)<2.1.

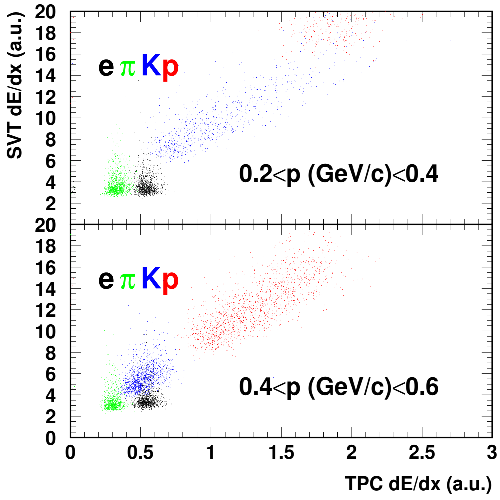

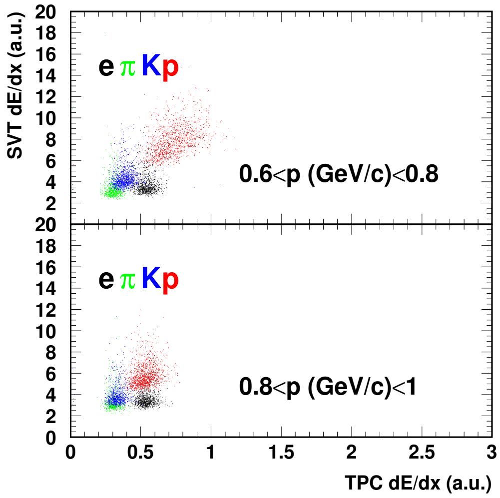

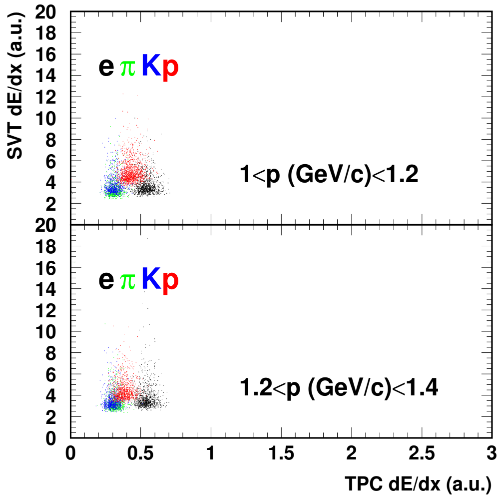

SVT dE/dx (a.u.)
e π K p
1<p (GeV/c)<1.2
1.2<p (GeV/c)<1.4
TPC dE/dx (a.u.)

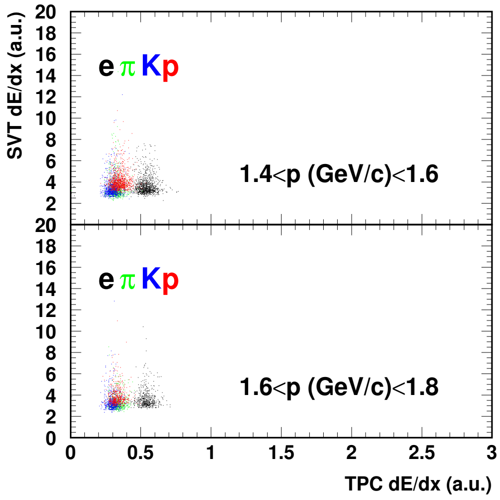

SVT dE/dx (a.u.)
e π K p
1.4<p (GeV/c)<1.6
1.6<p (GeV/c)<1.8
TPC dE/dx (a.u.)

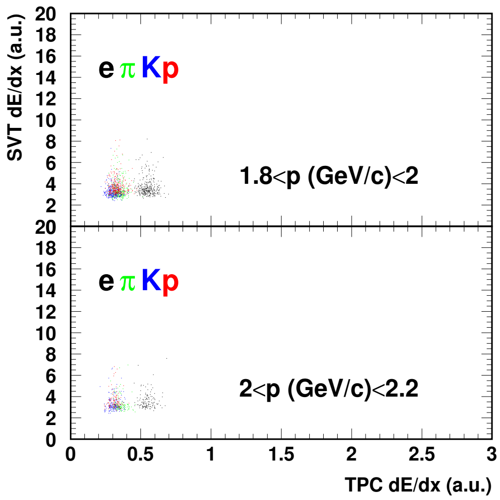
SVT dE/dx (a.u.)
e π K p
1.8<p (GeV/c)<2
e π K p
2<p (GeV/c)<2.2
TPC dE/dx (a.u.)